

IMPACT OF SURFACE VISCOSITY UPON AN ANNULAR MAGNETOHYDRODYNAMIC FLOW

Jules Delacroix, Laurent Davoust

*Grenoble Institute of Technology (Grenoble-INP), University of Grenoble Alpes, CNRS.
Materials & Processes Science & Engineering (SIMaP) Laboratory, Electromagnetic
Processing of Materials (EPM) Group, 38402 St-Martin d'Hères, France*

Using a matched asymptotic expansion based on the small parameter $1/\text{Ha}$, this paper addresses an original analytical coupling between surface rheology of, e.g., a gradually oxidizing liquid metal surface, and a supporting annular MHD flow. It is shown that the level of surface viscosity drives the electrical activation of the Hartmann layers, heavily modifying the MHD flow topology and leading to the emergence of a Lorentz force, for which the interaction with the flow is not classical. These analytical results are compared to a 2D numerical study, highlighting a fair agreement as soon as $\text{Ha} \geq 10$.

Introduction. In many industrial applications, there is a rising concern of how to model the interactions between an electrically conducting fluid and a second phase, when both of them are subjected to an external magnetic field. Typically, the issue of how a magnetohydrodynamic (MHD) flow with a liquid/gas interface is affected when oxidation occurs is of prime interest. It potentially affects many fields, such as metallurgy (stirring by bubble plumes in reactors [1]), microelectronics (MHD driven metal cooling processes [2]), or nuclear fusion technology (two-phase MHD issues with the breeder blanket based cooling loop [3]).

To our knowledge, little is actually known about the surface rheology of MHD flows, e.g., when a liquid metal is progressively contaminated through oxidation processes. On the one hand, the viscoelastic properties of liquid metals have been experimentally investigated [4], highlighting radically different mechanical behavior characteristics that depend on the level of oxidation, but those works are not related to MHD. On the other hand, the MHD of single-phase laminar flows exposed to strong uniform magnetic fields has been studied extensively for many years, for numerous layouts [5–7]. However, it seems that the fundamental issue of varying boundary conditions has been essentially considered from an electrical point of view. Thus, in the case of duct flows, the walls can have infinite electrical conductivity (see Shercliff [5]), no conductivity (Moreau [7]), mixed infinite and vanishing conductivities (Hunt *et al.* [6]), or arbitrary (Tabeling *et al.* [8]). The electrical influence of the walls, traduced by the ratio of bulk and wall electrical conductivities σ/σ_w , completely modifies the electrical circuit and results in a major impact on the topology of the MHD flow.

In this study, the same kind of general approach for the boundary condition is adopted, but this time from a mechanical point of view. In the light of what is previously enhanced, for flows including liquid/gas interfaces, the competition between bulk MHD and surface rheology (driven by the contamination rate of the liquid surface) may lead to a mechanically varying boundary condition. This change in liquid surface condition is suspected to affect greatly the overall MHD flow (see, e.g., the oscillatory flow patterns caused by surface oxidation described by Zhang *et al.* [9], in the case of a liquid metal subjected to a rotating magnetic field). To deal with the practical or industrial conditions, there is a need to inves-

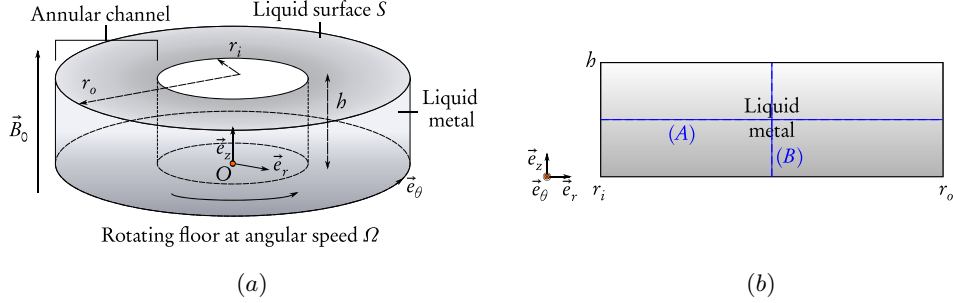


Fig. 1. Geometry under consideration. Note that (A): $z = h_0/2$ and (B): $r = (r_i + r_o)/2$ are cutting lines used for interpretation of the results.

tigate the surface mechanics separately from the bulk flow, especially, when the free surface is gradually oxidizing. Hence, the mechanics of a more or less oxidized interface coupled with an MHD liquid metal bulk is worthy of investigation, which is, to our knowledge, an original approach coupling both MHD and surface rheology.

1. Outlines. The system under consideration, the annular MHD viscometer, is displayed in Fig. 1. The problem is considered 2D axisymmetric ($\partial/\partial\theta = 0$), so that the domain can be reduced to the cross-section of the annular channel (Fig. 1b). The interest in this configuration, which is inspired by the deep channel viscometer [10–13], is that it is likely to generate strong velocity gradients along the \mathbf{e}_z -axis, whereas these gradients develop preferentially along the \mathbf{e}_r -axis in the more conventional case of the Taylor–Couette layout. As shown later in Eq. (8), the coupling term between the interface and the sub-phase flow brings a $\partial v_\theta/\partial z$ term into play, where v_θ is the azimuthal sub-phase velocity; the resulting shearing is expected to be more significant than in the Taylor–Couette layout, and the effects of varying boundary conditions at the liquid surface may be more easily highlighted. By considering the vertically applied magnetic field \mathbf{B}_0 , it can be demonstrated that the generating term for the azimuthal magnetic induction B_θ is $\partial v_\theta/\partial z$ as well (see Eq. (1)), which explains the interest in favoring gradients along \mathbf{e}_z .

The aim of this paper is to highlight the competitive effects between surface shearing and a strong transverse uniform magnetic field, especially, with the emergence of an electrically active Hartmann layer along a gradually denser liquid surface, e.g., under oxidation processes. For this purpose, two approaches are developed, i.e. an analytical method and a numerical modelling, both being based on a (\mathbf{v}, \mathbf{B}) formulation (see hereafter).

2. Mathematical model.

2.1. Bulk flow. Using the Maxwell and Navier–Stokes equations and assuming that the Reynolds number is low enough so that the inertial effects can be neglected, we can derive the following set of equations that governs the MHD problem and traduces the balance between electromagnetic and viscous effects (see, e.g., [6]), where the superscript ‘*’ refers to non-dimensional quantities:

$$\frac{\partial^2 B_\theta^*}{\partial r^{*2}} + \frac{1}{r^*} \frac{\partial B_\theta^*}{\partial r^*} - \frac{B_\theta^*}{r^{*2}} + \frac{\partial^2 B_\theta^*}{\partial z^{*2}} + \text{Ha} \frac{\partial v_\theta^*}{\partial z^*} = 0, \quad (1)$$

$$\frac{\partial^2 v_\theta^*}{\partial r^{*2}} + \frac{1}{r^*} \frac{\partial v_\theta^*}{\partial r^*} - \frac{v_\theta^*}{r^{*2}} + \frac{\partial^2 v_\theta^*}{\partial z^{*2}} + \text{Ha} \frac{\partial B_\theta^*}{\partial z^*} = 0, \quad (2)$$

Impact of surface viscosity upon an annular magnetohydrodynamic flow

with $r^* = r/h$, $z^* = z/h$, $v_\theta^* = v_\theta/\hat{V}$, $B_\theta^* = B_\theta/\hat{B}$, $\text{Ha} = B_0 h \sqrt{\sigma/\eta}$, and with $\hat{B} = \mu \hat{V} \sqrt{\sigma \eta}$, μ being the magnetic permeability of the fluid, and $\hat{V} = h\omega$, so that $v_\theta^*(r^*, z^* = 0) = r^*$ for the rotating floor. The associated boundary conditions are written as follows (see, e.g., [5] for the condition $B_\theta^* = 0$ all around the bulk flow):

$$v_\theta^*(r^* = r_i/h, z^*) = 0, \quad B_\theta^*(r^* = r_i/h, z^*) = 0, \quad (3)$$

$$v_\theta^*(r^* = r_0/h, z^*) = 0, \quad B_\theta^*(r^* = r_0/h, z^*) = 0, \quad (4)$$

$$v_\theta^*(r^*, z^* = 0) = r^*, \quad B_\theta^*(r^*, z^* = 0) = 0, \quad (5)$$

$$B_\theta^*(r^*, z^* = 1) = 0, \quad (6)$$

$$v_\theta^*(r^*, z^* = 1) = v_{\theta S}^*(r^*). \quad (7)$$

2.2. Surface flow. The boundary condition (7) brings a new unknown into play, which is the surface velocity $v_{\theta S}$. This stands as the first term of the two-way coupling between the surface and MHD bulk flow equations. The surface flow equation can be derived from a momentum balance written on an elementary heterogeneous volume that straddles a liquid surface of zero thickness (Gibb’s approach):

$$\text{Bo} \left(\frac{d^2 v_{\theta S}^*}{dr^{*2}} + \frac{1}{r^*} \frac{dv_{\theta S}^*}{dr^*} - \frac{v_{\theta S}^*}{r^{*2}} \right) = \left. \frac{\partial v_\theta^*}{\partial z^*} \right|_{z^*=1}. \quad (8)$$

Here, use is made of the surface “excess” viscous shear viscosity introduced by way of the Boussinesq–Scriven constitutive law (see, e.g., [14] for further details). The Boussinesq number $\text{Bo} = \eta_S/\eta h$ describes the balance between bulk (η is the Newtonian bulk shear viscosity) and surface (η_S is the surface excess shear viscosity along the liquid surface) viscous shearing. To solve for Eq. (8), also referred to as

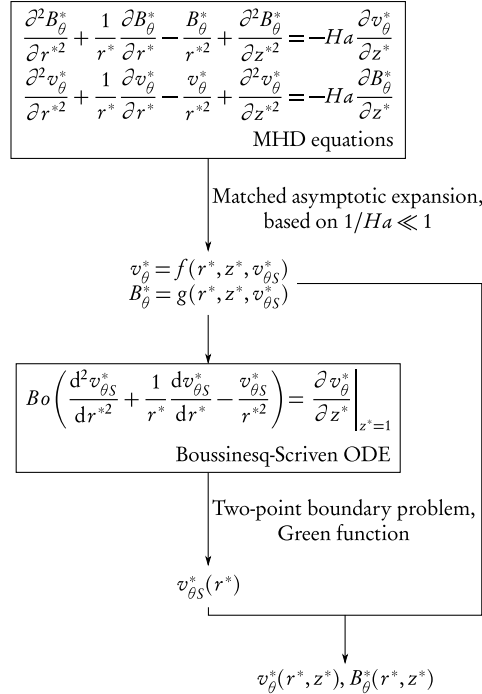


Fig. 2. Two-way analytical coupling between the bulk and surface flows [15].

the jump momentum balance (JMB), the following Dirichlet end-point boundary conditions are required:

$$v_{\theta S}^* \left(r^* = \frac{r_i}{h} \right) = 0, \quad v_{\theta S}^* \left(r^* = \frac{r_o}{h} \right) = 0. \quad (9)$$

2.3. Two-way analytical coupling. The overall coupling process between the sub-phase flow v_{θ}^* and the surface flow $v_{\theta S}^*$ stems from a somewhat tedious calculation process (summarized in Fig. 2), based on a matched asymptotic expansion for the bulk flow solution and on the determination of a Green function for calculating the surface velocity. Details of the calculations are available in a companion paper [15].

2.4. Numerical modelling. The previous analytical modelling derives from a matched asymptotic expansion based on the vanishing parameter $1/\text{Ha}$. Strictly speaking, these results are mathematically true when $\text{Ha} \rightarrow \infty$. However, in order to keep significant physical insight, a large range of values for Ha has been tested and interpreted, resulting in different MHD topologies. The interpretations stemming from this analysis must, therefore, be benchmarked to check how far they are relevant when Ha is only considered high enough (and not infinite). Consequently, there is a need for a method that circumvents the infinite Ha issue, even if the model must still conform to the assumption that the inertial terms are neglected.

Eqs. (1), (2) and (8), along with the boundary conditions (3), (4), (5), (6), (7) and (9) are discretised using the finite element method (FEM). A fully-coupled approach, which operates on the full Jacobian matrix as one entity, is implemented. This approach is based on the Newton–Raphson method, which linearises the non-linear problem based on the current solution, at each iteration. A linear stationary direct solver is implemented to solve for the linearised problem, i.e. the MULTifrontal Massively Parallel sparse direct Solver (MUMPS) based on LU factorisation (see MUMPS support [16] for further details). The computational domain is meshed with 18036 elements, mainly triangular, with a specific boundary layer mesh refinement at the boundaries of the fluid domain. The thickness of the first layer is carefully chosen so that the essential physics is captured.

3. Results and interpretations.

3.1. Analytical asymptotic results. In this section, the aim is to highlight two radically different MHD regimes and to see how the overall flow topology can be strongly modified by surface rheology through surface viscous shear. Consequently, only the asymptotic cases $\text{Ha} \gg \text{Bo}$ and $\text{Ha} \ll \text{Bo}$ are discussed.

If $\text{Ha} \gg \text{Bo}$, the v_{θ}^* contours demonstrate a 2D tendency with exclusively radial velocity gradients (apart near the side-walls), as seen in Fig. 3*a*. This rigid-body motion, traducing the electromagnetic blocking of the flow first observed by Lehnert [17], is caused by the well-known two-dimensionality tendency of magnetic induction. As a consequence, the interface is perfectly aligned with the bulk, and the bulk viscous shear at the interface is no longer significant. Therefore, the electric current density is found essentially vertical, closing up only inside the Shercliff layers (see Fig. 3*c*).

Now, when $\text{Ha} \ll \text{Bo}$, the results consist of a quite uniform “motionless” configuration, the momentum being mainly concentrated near the right corner at the bottom (Fig. 3*b*). This singular phenomenon is partially explained by the fact that, in this case, the surface dynamics is governed by surface viscous shear and behaves as a non-sliding membrane. Thus, v_{θ}^* must match with the vanishing component $v_{\theta S}^*$ at the surface. However, this cannot solely explain the motionless core across the whole cross-section. Other reasons can be found by focusing on the electric current densities. Due to strong velocity gradients near

Impact of surface viscosity upon an annular magnetohydrodynamic flow

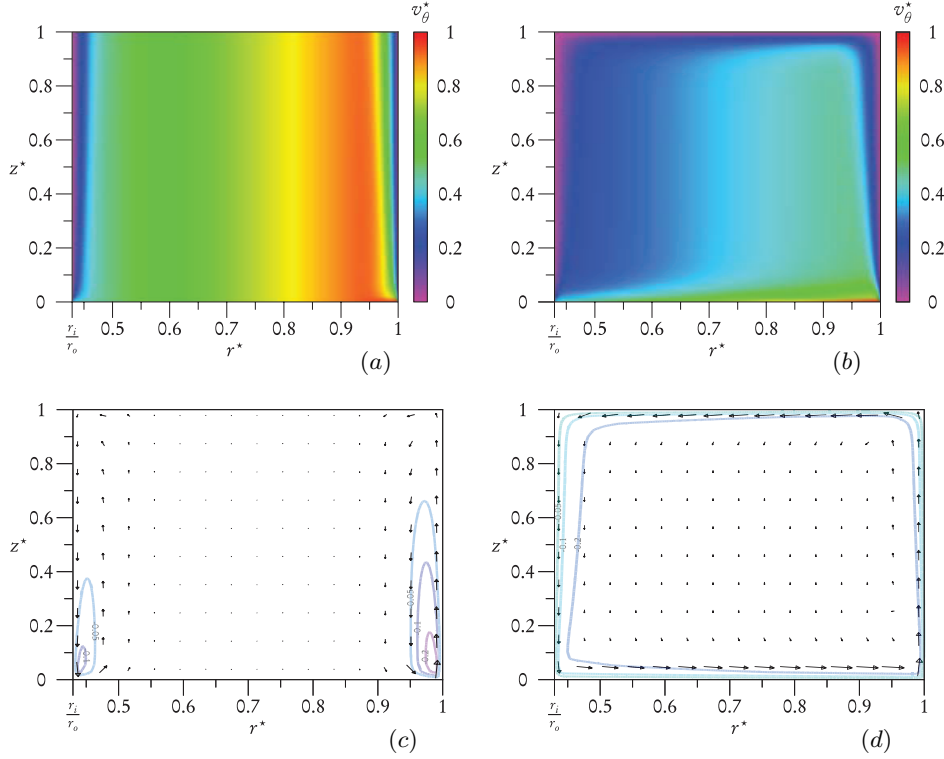


Fig. 3. Bulk MHD quantities for the two extreme cases $Bo \ll Ha$ (left-hand column) and $Bo \gg Ha$ (right-hand column). (a) and (b) represent v_θ^* , and (c) and (d) represent the vector current density \mathbf{j}^* with B_θ^* streamlines. For a given velocity $\Omega = 0.25$ rpm, with $r_0 = 7$ cm, $h = 1$ cm, $\sigma = 2.3 \times 10^6$ S·m $^{-1}$ and $\eta = 2.4 \times 10^{-3}$ N·m $^{-1}$, $\bar{J} = 4.1 \times 10^2$ A·m $^{-2}$ for $Ha = 30$ (right-hand side) and 6.8×10^2 A·m $^{-2}$ for $Ha = 50$ (left-hand side). \mathbf{j}^* is log-scaled by the magnitude $\exp\{(\ln(|\mathbf{j}|/|\mathbf{j}|_{\max})) / (1 + p)\}$, $p = 3$ for (c) and $p = 1$ for (d).

the liquid/gas surface and to current continuity, electric current densities are now found to flow within the top and bottom Hartmann layers, that are, therefore, electrically active (see Fig. 3d. The presence of a strong radial component of the electric current density, in combination with the imposed magnetic field $B_0 \mathbf{e}_z$, leads to the emergence of a Lorentz force $-j_r B_0$ along the azimuthal direction. As deduced from Fig. 3d, this Lorentz force is negative at the bottom and positive at the top of the channel cross-section. Consequently, this leads to an electromagnetic damping of the momentum injected from the rotating floor at the bottom, while it enhances the momentum in the upper part of the channel. Both contributions lead to a homogenization of the flow, which explains the overall flow patterns.

3.2. Numerical results. In order to compare analytical and numerical results, the velocity and electric current density profiles are displayed in Fig. 4, along the cutting lines (A) and (B) (defined in Fig. 1), allowing for the analysis of the MHD core flow and the Shercliff or Hartmann layers, respectively. Note that the radial component of electric current densities is several orders of magnitude lower than the axial component inside the Shercliff layers; the opposite situation holds inside the Hartmann layers, due to the current continuity. Consequently, the choice is made to plot only j_z^* along (A) and only j_r^* along (B).

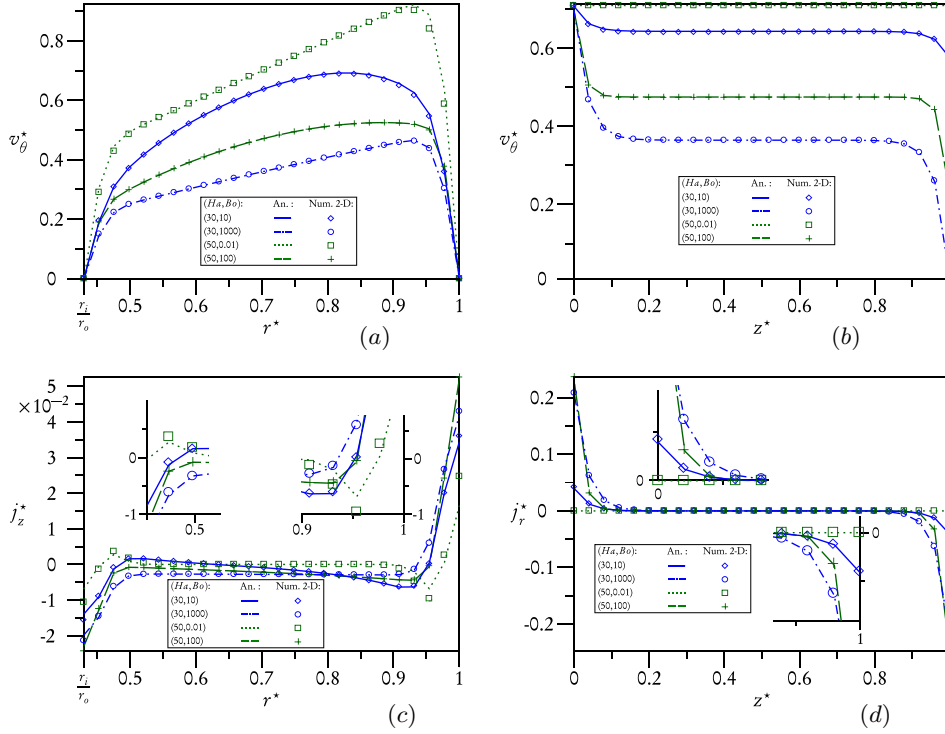


Fig. 4. Numerical (symbols) and analytical (lines) velocity and electric current density components along the cutting lines (*A*) (left-hand column) and (*B*) (right-hand column). The electric current densities are normalised with respect to the maximum electric current \bar{J}_{\max} reached for all cases, i.e. for $Ha = 50$, which corresponds to $\bar{J}_{\max} = 6.8 \times 10^2 \text{ A}\cdot\text{m}^{-2}$.

A quite satisfactory agreement between analytical and numerical results is achieved. Both models predict the same evolution with respect to the dimensionless numbers Ha and Bo . For the given Bo value, the flow evolves towards the rigid-body motion previously highlighted with the increasing Ha , causing the velocity to become independent of the axial coordinate, with an essentially axial electric current (curves (\dots) and (\square)). For the given Ha number, the electrical activation of the Hartmann layers with increasing Bo is obvious in Fig. 4*d*, and the motionless homogeneous flow topology dominates (Fig. 4*a,b*), as shown, for instance, by curves $(--)$ and $(+)$.

As previously said, the analytical calculation is based on the assumption $Ha \gg 1$, allowing for the matched asymptotic expansion to be performed. This stringent condition does not apply to the numerical modelling, as long as the inertial effects can be neglected. This is, therefore, interesting to determine the critical Ha value, at the onset of which the two methods show a significant discrepancy. For this purpose, v_θ^* and j_z^* profiles along (*A*) are displayed in Fig. 5 for several low Ha values at the given $Bo = 1$.

Concerning velocity, the discrepancy is hardly noticeable (Fig. 5*a*). A major difference consists of a non-vanishing velocity at the side walls for a very low $Ha = 2$ value (curves (\dots) and (\diamond)). This non-physical result (the side-walls being motionless) is explained by the fact that in the analytical study, the so-called inner corner regions have been left out of the reasoning. The typical cross-section of such

Impact of surface viscosity upon an annular magnetohydrodynamic flow

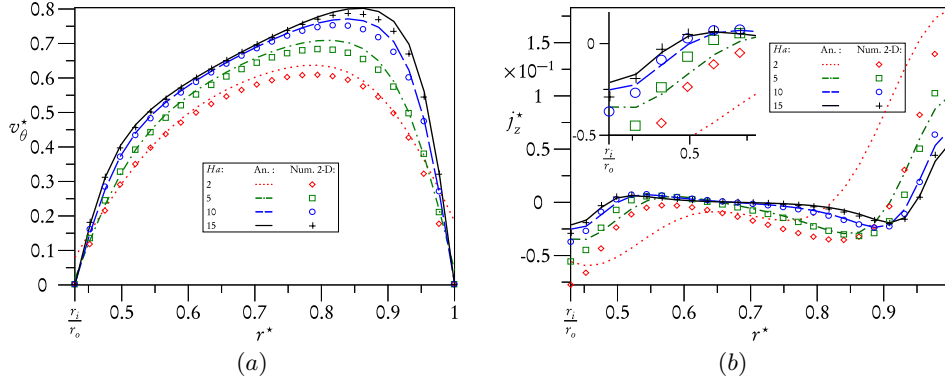


Fig. 5. Numerical (symbols) and analytical (lines) velocity and axial electric current density along the cutting line (A) for $Bo = 1$. The electric current densities are normalised with respect to the maximum electric current \bar{J}_{\max} reached for all cases, i.e. for $Ha = 15$, which corresponds to $\bar{J}_{\max} = 2 \times 10^2 \text{ A}\cdot\text{m}^{-2}$.

regions is $O(Ha^{-1}) \times O(Ha^{-1})$, which means that their influence on the flow is all the stronger with lower Ha values ($Ha = 2$ here).

The discrepancy is more obviously observed in Fig. 5b. For $Ha = 2$ (curves (\cdots) and (\diamond)) or $Ha = 5$ (curves $(-\cdot-)$ and (\square)), the results significantly differ from each other, whereas for $Ha = 10$ (curves $(--)$ and (\circ)) or $Ha = 15$ (curves $(-)$ and $(+)$), the agreement is quite satisfying. As a consequence, the value $Ha = 10$ can be proposed as a threshold, above which the matched asymptotic expansion proves relevant.

4. Conclusion. Based on both an original mathematical modelling and a numerical modelling, the coupling mechanisms between the rheology of a liquid surface and a supporting MHD bulk flow have been successfully investigated. The competitive effects of surface viscous shearing and electromagnetism have been highlighted: surface rheology is indeed found to monitor the generation of the Hartmann layers, leading, therefore, to a major change in the topology of the electrical circuit, which dramatically affects the overall MHD core flow. The comparison between the analytical and numerical results shows a good agreement and allows for the value $Ha = 10$ to be selected as the threshold value for the relevance of the matched asymptotic expansion.

Acknowledgements. This work was supported by a national grant from the French Ministry for Higher Education and Research.

REFERENCES

[1] J.W. HAVERKORT AND T.W.J. PEETERS. Magnetohydrodynamic effects on insulating bubbles and inclusions in the continuous casting of steel. *Metallurgical and Materials Transactions B*, vol. 41B (2010), pp. 1240–1246.

[2] T. LIU, P. SEN AND C.-J. KIM. Characterization of nontoxic liquid-metal alloy galinstan for applications in microdevices. *J. Microelectromechanical Systems*, vol. 21 (2012), pp. 443–450.

[3] N.B. MORLEY, S. SMOLENTSEV, L. BARLEON, I.R. KIRILLOV AND M. TAKAHASHI. Liquid magnetohydrodynamics: recent progress and future direc-

- tions for fusion. *Fusion Engineering and Design*, vol. 51–52 (2000), pp. 701–713.
- [4] V. KOLEVZON AND G. GERBETH. Light-scattering spectroscopy of a liquid gallium surface. *J. Phys. D: Appl. Phys.*, vol. 29 (1996), pp. 2071–2082.
- [5] J.A. SHERCLIFF. Steady motion of conducting fluids in pipes under transverse magnetic field. *Proc. Camb. Phil. Soc.* (Cambridge University Press, Cambridge), vol. 49 (1953), pp. 2071–2082.
- [6] J.C.R. HUNT AND K. STEWARTSON. Magnetohydrodynamic flows in rectangular ducts. ii. *J. Fluid Mech.*, vol. 23 (1965), pp. 563–581.
- [7] R. MOREAU. *Magnetohydrodynamics*. (Kluwer Academic Publishers, Dordrecht, 1990).
- [8] P. TABELING AND J.P. CHABRERIE. Magnetohydrodynamic secondary flows at high Hartmann numbers. *J. Fluid Mech.*, vol. 103 (1981), pp. 225–239.
- [9] CH. ZHANG, V. SHATROV, J. PRIEDE, S. ECKERT, AND G. GERBETH. Intermittent behaviour caused by surface oxidation in a liquid metal flow driven by a rotating magnetic field. *Metall. Mater. Trans. B*, vol. 42 (2011), pp. 1188–1200.
- [10] R.J. MANNHEIMER AND R.S. SCHECHTER. An improved apparatus and analysis for surface rheological measurements. *J. Colloid and Interface Science*, vol. 32 (1970), pp. 195–211.
- [11] A.H. HIRSA, J.M. LOPEZ, AND R. MIRAGHAIE. Determination of surface shear viscosity via deep-channel flow with inertia. *J. Fluid Mech.*, vol. 470 (2002), pp. 135–149.
- [12] L. DAVOUST, Y.-L. HUANG, AND S.-H. CHANG. Flow-induced melting of condensed domains within a dispersed Langmuir film. *Phys. Fluids*, vol. 20 (2008), 082105.
- [13] L. DAVOUST, Y.-L. HUANG, AND S.-H. CHANG. Shearing of a stratified layer of amphiphilic (bio)molecules. *Surf. Sci.*, vol. 603 (2009), 2777–2788.
- [14] J.C. SLATTERY, L. SAGIS AND E. OH. *Interfacial Transport Phenomena*. (Springer-Verlag, New York, 2007).
- [15] J. DELACROIX AND L. DAVOUST. Electrical activity of the Hartmann layers relative to surface viscous shearing in an annular magnetohydrodynamic flow. *Physics of Fluids*, vol. 26 (2014), 037102.
- [16] MUMPS SUPPORT. Multifrontal Massively Parallel Solver (MUMPS 4.10.0) User’s Guide. Technical report, ENS-Lyon and ENSEEIHT, 2011.
- [17] B. LEHNERT. An instability of laminar flow of mercury caused by an external magnetic field. *Proc. the Royal Society London A*, vol. 233 (1955), 299–302.

Received 06.01.2015